Available online at www.sciencedirect.com

SciVerse ScienceDirect

Ceramics International 38 (2012) 5369–5375

CERAMICS INTERNATIONAL

www.elsevier.com/locate/ceramint

Extension of Hasselman's thermal shock theory for crack/microstructure interactions in refractories

Vânia R. Salvini [a,*], Victor C. Pandolfelli [a], Richard C. Bradt [b]

[a] Federal University of São Carlos, Materials Engineering Department, GEMM, Via Washington Luiz, Km 235, São Carlos, SP, Brazil
[b] University of Alabama, Metallurgical and Materials Engineering Department, Tuscaloosa, AL, USA

Received 5 March 2012; received in revised form 18 March 2012; accepted 19 March 2012
Available online 27 March 2012

Abstract

Thermal shock damage resistance in advanced refractories depends on the crack interactions with the microstructure. These energy dissipation mechanisms during crack propagation are not directly considered in the original classical thermal shock model of Hasselman. They are imbedded within the N and γ terms of his derivations. In this extension of Hasselman's work, an expression is presented, which estimates the final crack size (ℓ_f) as the fracture surface energy ratio between γ_{NBT} and γ_{WOF}. That expression directly considers the crack interaction mechanisms with the refractory microstructure as it includes the R-curve behavior effects. In addition, the equation presented allows a quantitative evaluation of the volumetric density of cracks in refractories.
© 2012 Elsevier Ltd and Techna Group S.r.l. All rights reserved.

Keywords: Thermal shock damage; Refractories; Hasselman's energy balance model

1. Introduction

In recent years, novel microstructural classes of refractories have been developed in order to achieve improved performance in severe thermal mechanical conditions. In most cases, the analysis of these materials suggests that there is a strong interaction of the thermal shock induced cracks with the refractory microstructure. Usually, quasi-static or stable fracture occurs in these refractories, as it does in other materials that contain a high density of microcracks. This occurs because the stored elastic strain energy per unit volume is low and it is rapidly dissipated through the propagation of existing microcracks. The stored elastic strain energy release during the crack interaction with the microstructure of the refractory material directly influences the final crack length. Therefore, suitable equations that relate the residual mechanical strength and the volumetric crack density will be helpful for designing refractory compositions for application purposes. It is well known in both, the literature and from practical experience, the close relationship of the work of fracture (γ_{WOF}) and the energy for crack initiation (γ_{NBT}) ratio [1]. In general a high ($\gamma_{WOF}/\gamma_{NBT}$) ratio is attained for those refractories with a good thermal shock damage resistance. A good value for the ratio is $\geq$10, although much higher values can be obtained.

The classical mechanics model of Hasselman [2,3] assumes that the refractory material contains uniformly distributed defects. Hasselman derived the following general equation for thermal shock crack initiation (ΔT_C):

$$\Delta T_C = \left[\frac{\pi\gamma(1-2\nu)^2}{2\alpha^2 E(1-\nu^2)}\right]^{1/2} \cdot \left[1+\frac{16(1-\nu^2)N\ell^3}{9(1-2\nu)}\right] \cdot (\ell)^{1/2} \quad (1)$$

where E is the elastic modulus (GPa); N the volumetric initial density of cracks (1/cm^3); ℓ the crack length (m); α the linear thermal expansion coefficient ($^\circ$C^{-1}); ν the Poisson ratio and γ the fracture energy (J/m^2). The two terms N and γ are the factors which appear to be directly related to the refractory microstructure. Those two factors are the focus of this paper.

In his original derivation, Hasselman did not clearly specify the character of the fracture surface energy term. However according to his papers it is related to the effective surface energy of fracture. In Fig. 1 the solid curves represent Eq. (1) after Hasselman. At the time of Hasselman's papers, in the

* Corresponding author. Tel.: +55 16 33518253; fax: +55 16 33615404.
E-mail address: pvrs@ufscar.br (V.R. Salvini).

0272-8842/$36.00 © 2012 Elsevier Ltd and Techna Group S.r.l. All rights reserved.
doi:10.1016/j.ceramint.2012.03.046

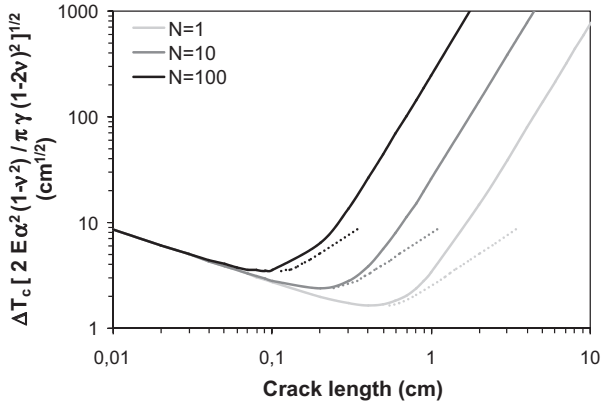

Fig. 1. Minimum thermal shock required to initiate the crack propagation as a function of the initial crack length ℓ_o and crack density N [2]. The dotted lines indicate the final crack lengths for each condition.

1960s, the concepts of fracture surface energy were not as well understood as they are today. Fracture mechanics was in its infancy and the concept of an *R*-curve was not yet known. In the mid-1900s, many believed that the fracture surface energy was equivalent to the thermodynamic surface free energy, only a few J/m^2. Today, almost half century since the appearance of Hasselman's first thermal shock paper, his original global energy concept of an effective surface energy remains valid. However, it is now realized that there are two important fracture surface energies. One is the energy for crack initiation ℓ and the other is that for crack propagation γ_{NBT}, the work of fracture. That is the origin of the ($\gamma_{WOF}/\gamma_{NBT}$) ratio.

When Nakayama [2] measured the work of fracture for refractories, there was surprise that the energy values were dozens of J/m^2, much greater than the thermodynamic surface free energy. When these were associated with fracture mechanics concepts, it became evident that although K_{IC} did correctly describe the initiation of fracture, most refractories had rising *R*-curves so that K_{IR} increased with crack extension, $\Delta\ell$ (Δa and Δc are also used). The existence of a rising *R*-curve is the reason that the work of fracture values are so much greater than the thermodynamic surface free energy for refractories. Fundamentally, it is the refractory microstructure/crack interactions that result in the rising *R*-curves and the large values of γ_{WOF}. The concept of a rising *R*-curve has never been satisfactorily introduced into the original Hasselman energy balance. It is a challenging task.

Moreover, Hasselman's theory demonstrates that for cracks which are initially short, then after their initiation the elastic energy is partly transformed into kinetic energy for crack growth. This means that the crack only reaches its final length when the release of the stored energy is equal to the total energy of the surface created. This energy balance condition is expressed in the Hasselman's Unified Theory of Thermal Shock [1] by his equation:

$$\frac{3}{2}\frac{(\alpha\Delta T_C)^2 E}{(1-2\nu)}\left\{\left[1+\frac{16(1-\nu^2)N\ell_0^3}{9(1-2\nu)}\right]^{-1}-\left[1+\frac{16(1-\nu^2)N\ell_f^3}{9(1-2\nu)}\right]^{-1}\right\}=2\pi N\gamma(\ell_f^2-\ell_0^2) \quad (2)$$

From rearranging and reformatting Eq. (2), the final crack length (ℓ_f) after thermal shock is expressed by:

$$\ell_f=\left[\frac{3(1-2\nu)}{8(1-\nu^2)N\ell_0}\right]^{1/2} \quad (3)$$

This final crack length is represented by the dotted lines in Fig. 1.

For those refractories which have a high internal density of cracks, thermal shock crack propagation usually occurs in the quasi-static mode. The energy-based interaction of these cracks with the microstructure of the material is represented by the work of fracture, γ_{WOF} [3,4] and express its influence in the rising *R*-curve behaviour. Therefore, Eq. (3) does not fully represent the values of ℓ_f nor final N for most refractory materials, although it usually describes the expected trends.

It must be appreciated that the basic principles of LEFM (linear elastic fracture mechanics) are not strictly adhered to by most industrial refractories [5]. Although most all glasses and structural ceramics are linearly elastic to fracture, industrial refractories invariably exhibit a readily observable non-elastic region prior to fracture during loading. The apparent elastic modulus is observed to decrease in this region. Because refractories are not perfectly linear elastic materials, some of the LEFM concepts such as K_{IC} are not applicable to refractories in the strictest sense. Generally the amount of inelastic behavior in refractories is a bit larger than the crack tip plasticity that occurs in most metals even though the principles of LEFM are still applicable to the metals. For this reason, although we are not ready to totally abandon LEFM in refractory problems, it suggests that there is considerable merit to and that it may be more appropriate to apply energy based concepts in a manner parallel to those applied by Hasselman to his original thermal shock damage assumptions to refractories.

In this paper, the two fracture surface energy based concepts of crack initiation energy, γ_{NBT}, as measured by the notched beam test and the crack propagation energy, γ_{WOF}, as determined by the total work to fracture in the chevron notched beam test, are utilized in place of the stress intensity factors K_{IC} and K_{IR}, as they relate to the crack initiation and the energy dissipation plateau conditions for the *R*-curves. A modified mathematical expression for the final crack length parameter is developed considering the balance between the two fracture surface energies γ_{NBT} and γ_{WOF}. This successfully reflects the rising *R*-curve. This approach expands the applicability of Hasselman's general unified theory. The results are then applied to estimate the final volumetric crack density (N_f) as a function of experimental thermal shock damage (ΔT) for five specifically designed refractories in the Al_2O_3–$3Al_2O_3{\cdot}2SiO_2$–ZrO_2 system.

2. Materials and techniques

In order to specifically investigate the role of increasing the crack density of the refractory on the thermal shock damage of commercial refractories, a series of high alumina refractories were prepared with increasing microcrack densities. This was accomplished by incrementally adding greater amounts of an aggregate with a significantly different coefficient of thermal expansion. The choices were an alumina matrix refractory composition with additions of a fused mullite–zirconia aggregate. There is precedence for this type of technical approach for a more thermal shock damage industrial refractory development. Miller et al. [6] have added zirconia to a dolomite, Ugaki et al. [7] have added aragonite to a dolomite and in a separate paper Uzaki et al. [8] have added an aggregate, most likely zirconia, to a mag-chrome refractory. Although this concept has not been previously applied to an alumina refractory, it is an obvious route to induce microcracking into almost any industrial refractory body. All of the above have achieved a microcracked refractory with enhanced thermal shock damage resistance. Unfortunately, these studies did not sufficiently characterize the refractories to enable the determination of crack densities.

Table 1 presents the five refractory formulations that were prepared for study with a tabular alumina T-60 (2–0.044 mm, Almatis, Germany), a calcined alumina APC-2011SG (<0.010 mm, Alcoa, Brazil) and a fused mullite–zirconia aggregate (1–0.21 mm, Showa Denko, Japan). The objective of adding the coarser mullite–zirconia aggregate to the refractory composition is to induce microcracks to provide a higher crack propagation resistance and to lower the thermal expansion coefficient, therefore generally improving the thermal shock performance for these alumina based refractories.

After mixing the above compositions, pressing at 23 MPa and sintering at 1510 °C for 12 h in air, prismatic samples (160 mm × 40 mm × 40 mm) were obtained for property measurements including mechanical and thermal shock evaluations.

2.1. Property measurements

Although many researchers use a single test sample, the work of fracture and notched beam tests were carried out on separate specimens for the two fracture energy measurements in this study [9]. The critical stress intensity factor (K_{IC}), using the single edge notched beam technique (SENB) (ASTM E-399), was determined at room temperature in a three-point bend test applying the following equation:

$$K_{\mathrm{IC}} = \sigma_f \sqrt{\pi \ell} \cdot A_i \tag{4}$$

where $\sigma_f = 3PL/2bh^2$ and $A_i = A_0 + A_1(\ell/h) + A_2(\ell/h)^2 + A_3(\ell/h)^3 + A_4(\ell/h)^4$. P is the applied load for crack initiation; L the span; ℓ the notch depth; h the sample thickness; b the sample width; ℓ; $A_0 = 1.90 + 0.0075(L/h)$; $A_2 = 15.4 - 0.2175(L/h)$; $A_3 = -26.24 + 0.2815(L/h)$ and $A_4 = 26.28 - 0.145(L/h)$.

The prismatic samples were center-notched to one-half of their thickness ($c/h \approx 0.5$) with a 0.3 mm thick diamond blade for the K_{IC} measurements. All fracture energy tests and cold modulus of rupture (MOR) were performed on Instron 1127 machine in three-point bending over a span of 140 mm. For K_{IC}, fracture surface energy (γ_{NBT}) and MOR, measurements were carried out at crosshead speed of 2 mm/min.

This measured value of K_{IC} was used to calculate the energy for crack initiation γ_{NBT} by the following expression:

$$K_{\mathrm{IC}} = (2\gamma_{NBT}E)^{1/2} \tag{5}$$

where E is Young's elastic modulus measured by a sonic technique on V-Meter C-4901 (James Instruments). Further details about this technique can be found in reference [10].

The γ_{NBT} represents the fracture surface energy to initiate crack propagation, whereas the work-of-fracture γ_{WOF} expresses the energy to propagate a crack through the specimen thickness. For the γ_{WOF} measurements, the samples were center-notched with a 0.3 mm thick diamond blade so that a chevron-shaped fracture cross section remained. The γ_{WOF} samples were loaded in 3 point bending at a crosshead speed of 0.01 mm/min to insure fully stable crack propagation. The γ_{WOF} values were then calculated by:

$$\gamma_{WOF} = \frac{\int F\,dx}{2A} \tag{6}$$

where $\int F\,dx$ represents the required work for new surfaces generation and A is the projected area of the new fracture surfaces as determined directly from the individual specimen chevron areas.

2.2. Mathematical approach

Hasselman's mathematical expression for the final crack length parameter ℓ_f was extended to include both γ_{NBT} and γ_{WOF} according to the following sequence of mathematical steps.

I. The difference between the required energy to initiate the crack extension (γ_{NBT}) and work of fracture (γ_{WOF}) was

Table 1
Refractory compositions.

	Composition				
	A	*B*	*C*	*D*	*E*
Tabular alumina T-60 (2–0.044 mm)	90	80	70	60	50
Calcined alumina APC-2011SG (<0.010 mm)	10	10	10	10	10
Mullite–zirconia aggregate (1–0.21 mm)	–	10	20	30	40

introduced into Eq. (1). Incorporating these terms, Eq. (2) can be rewritten as:

$$\frac{3}{2}\frac{(\alpha\Delta T_C)^2 E}{(1-2\nu)}\left\{\left[1+\frac{16(1-\nu^2)N_i\ell_0^3}{9(1-2\nu)}\right]^{-1}-\left[1+\frac{16(1-\nu^2)N_f\ell_f^3}{9(1-2\nu)}\right]^{-1}\right\}=2\pi N_f\gamma_{WOF}\ell_f^2-2\pi N_i\gamma_{NBT}\ell_0^2 \quad (7)$$

To further address the specific refractories, the following assumptions were made:

$$B_1=\frac{3}{2}\frac{(\alpha\Delta T_C)^2 E}{(1-2\nu)} \quad (8)$$

$$B_2=\frac{16(1-\nu^2)N_i}{9(1-2\nu)} \quad (9)$$

$$B_3=\frac{16(1-\nu^2)N_f}{9(1-2\nu)} \quad (10)$$

$$B_4=2\pi N_f\gamma_{WOF} \quad (11)$$

$$B_5=2\pi N_i\gamma_{NBT} \quad (12)$$

After incorporating these B_i terms, Eq. (7) is then expressed as:

$$B_1[(1+B_2\ell_0^3)^{-1}-(1+B_3\ell_f^3)^{-1}]=B_4\ell_f^2-B_5\ell_0^2 \quad (13)$$

II. For initially short cracks, where ℓ_0 is small and $\ell_f \gg \ell_0$, the following terms will be assumed to be small and near to zero, therefore they will be treated as zero for further mathematical applications of the equations:

$$B_5\ell_0^2\cong 0 \quad (14)$$

$$B_2\ell_0^3\cong 0 \quad (15)$$

$$\frac{1}{1+B_3\ell_f^3}\cong 0 \quad (16)$$

This enables one to reduce Eq. (13) to:

$$B_1=B_4\ell_f^2 \quad (17)$$

This significantly simplifies the aforementioned Eqs. (7) and (13), resulting in the following:

$$\ell_f=\left(\frac{B_1}{B_4}\right)^{1/2}=\left[\left(\frac{3(\alpha\Delta T_C)^2 E}{2(1-2\nu)}\right)\cdot\left(\frac{1}{2\pi N_f\gamma_{WOF}}\right)\right]^{1/2} \quad (18)$$

III. Considering the equation for the critical temperature difference (ΔT_C) to initiate the propagation of short cracks and assuming this γ value to be γ_{NBT}, results in:

$$\Delta T_C=\left[\frac{\pi\gamma_{NBT}(1-2\nu)^2}{2E\alpha^2(1-\nu^2)\ell_0}\right]^{1/2} \quad (19)$$

Substituting Eq. (19) into Eq. (18) yields:

$$\ell_f=\left[\left(\frac{\gamma_{NBT}}{\gamma_{WOF}}\right)\frac{3(1-2\nu)}{8(1-\nu^2)}\frac{1}{N_f\ell_0}\right]^{1/2} \quad (20)$$

Eq. (20) can be applied to consider the crack interaction with the microstructure in determination of the final crack length, ℓ_f, as it contains the ratio ($\gamma_{NBT}/\gamma_{WOF}$). It also describes the K_{IR} of the *R*-curve plateau. In case of flat *R*-curve materials, such as glass and some fine grain size structural ceramics, there is not any crack interaction with the microstructure ($\gamma_{NBT}=\gamma_{WOF}$) and Eq. (20) reduces to Eq. (3), as originally derived by Hasselman.

The final volumetric density of cracks (N) can be estimated by rearranging Eq. (20):

$$N_f=\left[\left(\frac{\gamma_{NBT}}{\gamma_{WOF}}\right)\frac{3(1-2\nu)}{8(1-\nu^2)}\frac{1}{\ell_f^2\ell_0}\right]^{1/2} \quad (21)$$

To calculate the crack density N_f, $\nu=0.20$, ℓ_0, the initial crack length before the thermal shock and ℓ_f, the final crack length after a single thermal shock ($\Delta T=500$, 800 and 1100 °C) were considered. Both ℓ_0 and ℓ_f, were obtained by applying Griffith's equation from the specimen strength measurements based on Eq. (4).

3. Results and discussions

3.1. Microstructural considerations

The ternary phase diagram for the Al_2O_3–ZrO_2–SiO_2 system is shown in Fig. 2. Point A refers to the chemical composition of the fused mullite–zirconia aggregate and points 1, 2 and 3 indicate the crystallization path as below:

- in the temperature range between 1900 °C and 1850 °C (path 1) the crystallization and the grain growth of primary ZrO_2 occurs;
- below ~1850 °C, path 2 leads to the formation of a columnar eutectic mullite–zirconia.

The optical micrograph of composition *C* in Fig. 3 illustrates the primary ZrO_2 grains (region 1), the mullite–zirconia eutectic (region 2) and the ternary eutectic compound ($3Al_2O_3{\cdot}2SiO_2$–SiO_2–ZrO_2) (region 3).

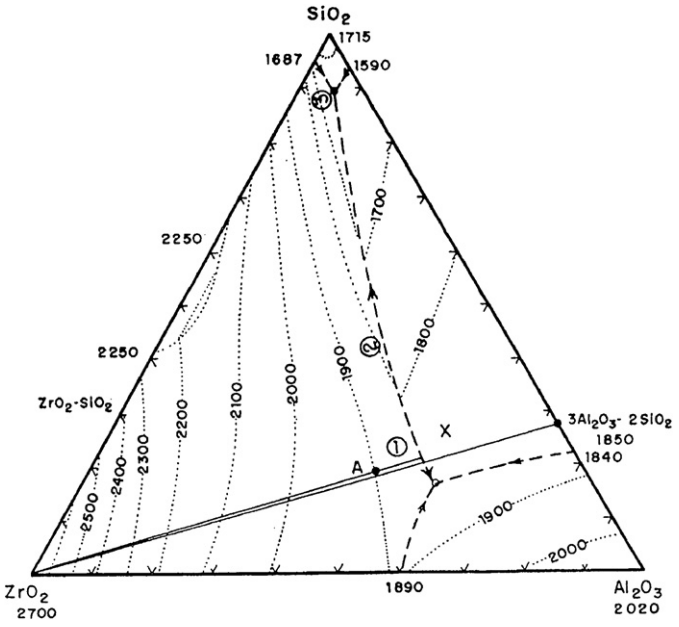

Fig. 2. Ternary phase diagram of Al_2O_3–ZrO_2–SiO_2 system: point A corresponds to the chemical composition of mullite–zirconia aggregate and, the paths 1, 2 and 3 indicate its crystallization path [11].

Based on visual fracture surface observations, the thermal shock crack propagation was transgranular for the mullite–zirconia aggregates. Some crack branching can be detected as shown in Fig. 4, where besides the main fracture, lateral cracks can also be seen. This may be a contributing factor for the γ_{WOF} increase for those compositions where crack coalescence was not verified. In Fig. 4, besides the columnar zirconia in the eutectic composition, primary zirconia pull-out can also be detected from the thermal expansion mismatch between the zirconia and the host phase.

3.2. Evaluation of the thermo mechanical properties

Table 2 summarizes the measured thermo mechanical properties (α, E, σ_f, K_{IC}, γ_{NBT} and γ_{WOF}) and the retained MOR

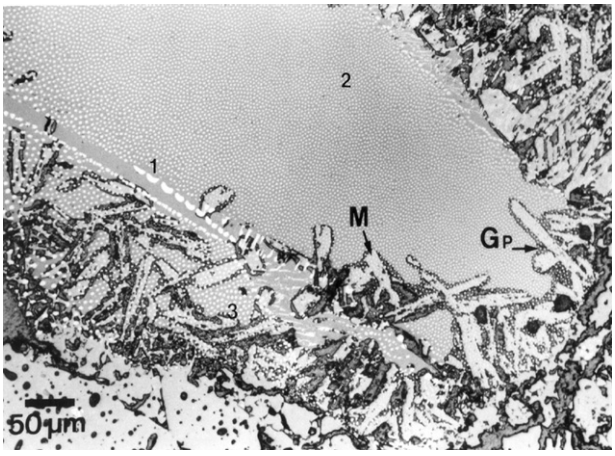

Fig. 3. Optical micrograph of the polished surface of composition C (20 wt.% of mullite–zirconia aggregate), where M and G_P refer to mullite and glassy phase, respectively. Regions 1, 2 and 3 indicate the crystallization path in the Al_2O_3–ZrO_2–SiO_2 phase diagram of as shown in Fig. 2.

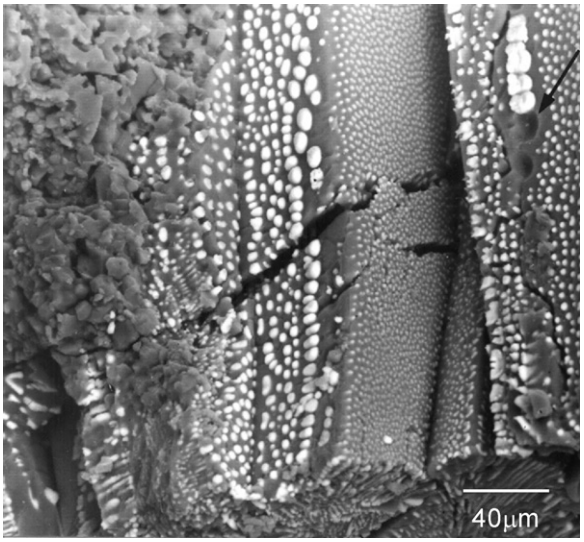

Fig. 4. Fracture surface of composition E highlighting the fused mullite–zirconia aggregate before thermal shock. The main crack and side ones (branching) can be detected and also a primary zirconia pull-out (indicated by arrow).

(strengths) of the refractory compositions after a single thermal shock of $\Delta T = 1100\ ^{\circ}C$ from a furnace into RT water.

Firstly addressing the fracture energy results (γ_{NBT} and γ_{WOF}), Table 2 reveals that γ_{NBT} attained a maximum value in the range of about a 10–20 wt.% mullite–zirconia aggregate addition. The γ_{WOF} increased in the range from 10 to 30 wt.% of the same aggregate. The γ_{WOF} is consistently much greater than the γ_{NBT}. The ratio of ($\gamma_{NBT}/\gamma_{WOF}$) ranges from 0.21 for the pure alumina to 0.59 for the highest mullite–zirconia content. These are typical ratios, but not quite as good as the very best observed for some advanced refractories (<0.10). When one considers the ratio ($\gamma_{NBT}/\gamma_{WOF}$) values in Table 2 and using Eq.(21), it is possible to estimate the density of cracks (N) as a function of the thermal shock severity (ΔT), as presented in Fig. 5.

Two important features are evident in the results presented in Fig. 5. Firstly, the influence of the addition of mullite–zirconia aggregate on the crack density, and, secondly, the crack density

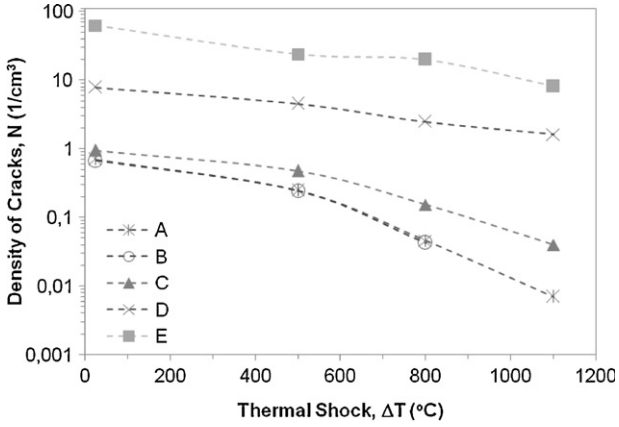

Fig. 5. The calculated final crack density (N_f) as a function of thermal shock severity (ΔT) for the five refractory compositions in Table 2, based on Eq. (21).

Table 2
Thermo mechanical properties of compositions.

	Composition				
	A	*B*	*C*	*D*	*E*
MZ aggregate[a] (wt.%)	0	10	20	30	40
α (10^{-6} °C^{-1})	8.14	7.75	8.30	6.69	5.18
E (GPa)	82.6± 0.1	87.5 ± 0.1	52.3 ± 0.1	27.8 ± 0.1	22.2 ± 0.1
σ_f (MPa)	14.1 ± 1.8	21.9 ± 0.4	17.6 ± 1.5	14.7 ± 0.4	13.9 ± 1.7
K_{IC} (MPa m$^{1/2}$)	1.58 ± 0.05	2.71 ± 0.34	2.04 ± 0.18	1.18 ± 0.07	0.93 ± 0.06
γ_{NBT} (J/m^2)	15 ± 0.8	43 ± 10	40 ± 7	25 ± 3	20 ± 3
γ_{WOF} (J/m^2)	73 ± 15	112 ± 8	118 ± 3	110 ± 4	34 ± 13
($\gamma_{NBT}/\gamma_{WOF}$)	0.21	0.38	0.34	0.23	0.59
MOR[b] (%)	27 ± 3	36 ± 5	44 ± 8	71 ± 3	62 ± 3

[a] Fused mullite–zirconia aggregate content.
[b] Retained MOR after a single thermal shock of $\Delta T = 1100$ °C.

changes with the severity of thermal shock for the five different refractory compositions.

Regarding the first point, in general the initial crack density increases with the increasing aggregate content in the refractory composition. This is a direct consequence of the microcrack generation within the material by the mullite–zirconia aggregates which have a lower coefficient thermal expansion than the alumina matrix. This is also confirmed by the decreasing E and σ_f with the mullite–zirconia aggregate content, although the later will also depend on the individual crack sizes and probably the interaction of adjacent microcracks within the refractory structures.

Concerning the second, the crack density decreases with the thermal shock severity ($>\Delta T$), perhaps due to the coalescence of the cracks during propagation. This trend is most interesting for compositions containing 10 and 20 wt.% of mullite–zirconia, those with the lower MOR (%) results. By contrast, those refractories with 30 wt.% of aggregate exhibited a lower rate of crack coalescence, matching with the results presented in Table 2, where this composition presented the least damage after the $\Delta T = 1100$ °C thermal shock.

Table 3 presents calculated values of volumetric crack density (N_f) as a function of a thermal shock. These were calculated by two different methods:

- Method 1 uses Eq. (21) as presented in this paper and,
- Method 2 refers to the Eq. (3) from Hasselman's original theory.

Regardless of the chosen method for calculating the crack densities, the obtained N_f values present the same trends as a function of mullite–zirconia content and thermal shock severity. However, the N_f values are always higher when Eq. (3) after Hasselman is used. This difference in values for N_f is a consequence of applying the ratio ($\gamma_{NBT}/\gamma_{WOF}$) in Eq. (21), which for well-designed refractories is always much less than unity because γ_{WOF} is higher than γ_{NBT}. Considering the previous aspect, the authors believe that the N_f values obtained by Eq. (21) may be more appropriate, because the ($\gamma_{NBT}/\gamma_{WOF}$) ratio more realistically expresses the mechanisms of crack interaction with the microstructure in the refractories.

Table 3
Crack density (N_f) as a function of thermal shock severity (ΔT) for composition *E*.

ΔT (°C)	Method 1 (1/cm^3)	Method 2 (1/cm^3)
Composition *E*		
0	62.4	106.7
500	23.9	40.9
800	19.9	34.1
1100	8.1	13.9

4. Conclusions

Based on the results, there is an increase of volumetric density of cracks (N) as a consequence of adding the fused mullite–zirconia aggregate into a refractory composition. A reduction in N values due to the apparent coalescence of cracks when the thermal shock was more severe was observed. The N values obtained using the equation presented in this paper appear to be more realistic, because the ratio $\gamma_{NBT}/\gamma_{WOF}$ expresses the different mechanisms of crack interaction with the microstructure of the refractory material. Additionally, for a given initial value of the crack density, the forecast residual strength based on the ℓ_f attained is closer to the experimental results and more helpful for designing purposes.

Acknowledgements

The authors are grateful to CNPq and FAPESP for financial support given during the development of the present work.

References

[1] D.P.H. Hasselman, Unified theory of thermal shock fracture initiation and crack propagation in brittle ceramics, J. Am. Ceram. Soc. 52 (11) (1969) 600–604.
[2] J. Nakayama, H. Abe, R.C Bradt, Crack stability in the work-of-fracture test: refractory applications, J. Am. Ceram. Soc. 64 (11) (1981) 671–675.
[3] J.J. Uchno, R.C. Bradt, D.P.H. Hasselman, Fracture surface energies of magnesite refractories, Am. Ceram. Soc. Bull. 55 (7) (1976) 665–668.
[4] R.C. Bradt, Elastic properties of refractories: their roles in characterization, Refractory Appl. 12 (3) (2007) 11–26.

[5] O.P.H. Hasselman, Elastic energy at fracture and surface energy as design criteria for thermal shock, J. Am. Ceram. Soc. 46 (11) (1963) 535–540.

[6] T. Miller, D. Griffin, S. Ishii, H. Kusunose, The development and use of dolomite–zirconia brick in cement rotary kilns, in: Proceedings of 2nd International Conference on Refractories, Tokyo, (1987), pp. 609–622.

[7] N. Ugaki, N. Chatni, Tsuchiya, et al., Thermal shock resistance of aragonite added magnesia-dolomite refractories for cement kiln, in: Proceedings of the 5th Symposium on refractories for cement industry in Japan, 1989, pp. 26–36.

[8] N. Uzaki, H. Ishii, K. Aratani, et al., Development of magnesite–chrome refractories with high thermal shock resistance, Interceram 40 (5) (1991) 279–283.

[9] D.R. Larson, J.A. Coppola, D.P.H. Hasselmans, R.C. Bradt, Fracture toughness and spalling behavior of high-Al_2O_3 refractories, J. Am. Ceram. Soc. 57 (10) (1974) 417–421.

[10] M. Sakai, R.C Bradt, Fracture toughness testing of brittle materials, Int. Mater. Rev. 38 (2) (1993) 53–78.

[11] M.C. Greca, J.V. Emiliano, A.M. Segadaes, Revised phase equilibrium relationships in the system Al_2O_3–ZrO_2–SiO_2, J. Eur. Ceram. Soc. 9 (1992) 271–283.